Electric-field-induced localisation of type-II coupled quantum wells

1990 J. Phys.: Condens. Matter 2 5723

(http://iopscience.iop.org/0953-8984/2/26/008)

J. Phys.: Condens. Matter 2 (1990) 5723–5728. Printed in the UK

Electric-field-induced localisation of type-II coupled quantum wells

Guoyi Qin
Centre for Theoretical Physics, The Laboratory of Solid State Microstructures, Nanjing University, Nanjing 210008, People's Republic of China

Received 31 October 1989, in final form 14 March 1990

Abstract. The asymptotic transfer method was used to calculate the electron energy spectra, electron envelope functions and the dispersion relations of type-II semiconductor coupled quantum wells when an electric field was applied along the growth axis. It turned out that the energy spectra were nearly evenly spaced. The electron envelope functions displayed strong localisation and the dispersion relations showed a non-parabolic shape.

1. Introduction

In [1], we suggested that the asymptotic transfer method (ATM) be used to calculate the electron sub-bands and envelope functions of a semiconductor system in which the band edges of both conduction band (CB) and valence band (VB) were not flat.

As an illustrative example, we performed there a self-consistent calculation of electron sub-bands and envelope functions of a type-I $Ga_{1-x}Al_xAs$ sawtooth superlattice taking account of the variation in effective mass of electrons with the concentration of Al.

When an electric field was applied along the growth axis, electron energy spectra and electro-optical properties of type-I semiconductor coupled quantum wells (CQWs) were discussed in [2] within the framework of the tight-binding description. To check the accuracy of this approach, they solved the Schrödinger equation for the single-band envelope function at the same time, but this is possible only when the electric potential was approximated by a piecewise-constant potential and the interaction between CB and VB was neglected.

Obviously by means of ATM, it is possible to take the declination of the edges of both CB and VB, as well as the interaction between CB and VB into account at the same time.

In section 2, we simply reviewed the ATM and generalised it to suit finite systems. Then, as the first example of a type-II system that ATM was used for, we discuss the properties of a finite set of type-II CQWs. In section 3, the results of numerical calculations for electron energy spectra, envelope functions and dispersion relations were given followed by a brief discussion.

2. Theory

The finite set of CQWs consists of N coupled quantum wells embedded between thick barriers with the same width and terminated by barriers that have finite widths at both

0953-8984/90/265723 + 06 $03.50

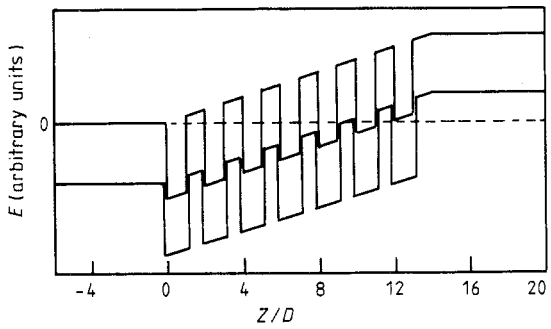

Figure 1. The sketch of a finite set of type-II InAs/GaSb CQWs that consists of seven CQWs.

ends. When an electric field is applied along the growth axis Z, the edges of both CB and VB are declined as sketched in figure 1.

If the electric field is not very strong, the lifetime of the carriers will be long, and the barriers at both ends can be approximated by barriers that are infinite in width and constant in height. The zero point of energy is chosen to be situated at the conduction band edge of the infinite barrier on the left-hand side.

The total length of CQWs located between the infinite barriers at both ends is L. The length L can be divided into j sublayers. If j is large enough, the width of each sublayer is very small. Within each sublayer, the lth sublayer for instance, the edges of both CB and VB can be considered approximately as constant V_s^l and V_p^l. The whole infinite barrier on the left-hand side can be considered as one sublayer and labelled as the zeroth sublayer, the sublayer next to it as the first sublayer and so forth. Using the method presented in [1], the amplitudes of the lth sublayer can be connected to that of the $(l+1)$th sublayer via a transfer matrix $\mathbf{T}_l$:

$$\begin{bmatrix} \tilde{A}_1^{l+1} \\ \tilde{B}_1^{l+1} \\ \tilde{B}_2^{l+1} \\ \tilde{A}_2^{l+1} \end{bmatrix} = \mathbf{T}_l \begin{bmatrix} \tilde{A}_1^{l} \\ \tilde{B}_1^{l} \\ \tilde{B}_2^{l} \\ \tilde{A}_2^{l} \end{bmatrix}. \tag{1}$$

Let $K_y = 0$, $K_\perp = K_x + iK_y = K_x$, then we have

$$\mathbf{T}_l = \begin{bmatrix} J_l \exp(i\alpha_l d_l) & \theta_l \exp(-i\alpha_l d_l) & -R_l \exp(-i\alpha_l d_l) & -R_l \exp(i\alpha_l d_l) \\ \theta_l \exp(i\alpha_l d_l) & J_l \exp(-i\alpha_l d_l) & R_l \exp(-i\alpha_l d_l) & R_l \exp(i\alpha_l d_l) \\ -R_l \exp(i\alpha_l d_l) & -R_l \exp(-i\alpha_l d_l) & J_l \exp(-i\alpha_l d_l) & \theta_l \exp(i\alpha_l d_l) \\ R_l \exp(i\alpha_l d_l) & R_l \exp(-i\alpha_l d_l) & \theta_l \exp(-i\alpha_l d_l) & J_l \exp(i\alpha_l d_l) \end{bmatrix} \tag{2}$$

where

$$J_l = \tfrac{1}{2}[(\alpha^R/M^R)^{1/2} + (M^R/\alpha^R)^{1/2}] \tag{3}$$

$$\theta_l = \tfrac{1}{2}[(\alpha^R/M^R)^{1/2} - (M^R/\alpha^R)^{1/2}] \tag{4}$$

$$R_l = \tfrac{1}{2}[K_\perp/(2\alpha_l\alpha_{l+1})^{1/2}][(1/M^R)^{1/2} - (M^R)^{1/2}] \tag{5}$$

in which

$$\alpha^R = \alpha_{l+1}/\alpha_l \qquad M^R = M^{l+1}/M^l \tag{6}$$

$$M^l = (\varepsilon_g^l + \varepsilon - V_p^l) \tag{7}$$

$$\alpha_l^2 = -(3/2\Pi^2)(\varepsilon_g^l + \varepsilon - V_p^l)(V_s^l - \varepsilon) - K_\perp^2. \tag{8}$$

In equations (3)–(8), Π is the Kane matrix element:

$$\Pi = (\hbar/m_0)\langle iS|\hat{p}_Z|Z\rangle. \tag{9}$$

ε_g^l is the energy gap of the lth sublayer, and V_s^l and V_p^l are the energy values of the conduction band edge and valence band edge of the lth sublayer, respectively. $\boldsymbol{K}_\perp$ is the wavevector in the plane perpendicular to the Z axis.

Because the wavefunctions must be bounded, the amplitudes of the exponentially increased waves in both infinite barriers must be zero, i.e.

$$\tilde{B}_1^{j+1} = \tilde{B}_2^{j+1} = \tilde{A}_1^0 = \tilde{A}_2^0 = 0. \tag{10}$$

Then by means of the successive product of $j+1$ transfer matrices, we obtain

$$\begin{bmatrix} \tilde{A}_1^{j+1} \\ 0 \\ 0 \\ \tilde{A}_2^{j+1} \end{bmatrix} = \prod_{l=0}^{j} T_l \begin{bmatrix} 0 \\ \tilde{B}_1^0 \\ \tilde{B}_2^0 \\ 0 \end{bmatrix}. \tag{11}$$

To simplify the calculation, a unitary transformation is made using the transformation matrix $\mathbf{U}$ [3]:

$$\mathbf{U} = \begin{bmatrix} (1/\sqrt{2})\exp(-i\varphi) & 0 & 0 & -(1/\sqrt{2})\exp(i\varphi) \\ 0 & (1/\sqrt{2})\exp(-i\eta) & -(1/\sqrt{2})\exp(i\eta) & 0 \\ 0 & (1/\sqrt{2})\exp(-i\eta) & (1/\sqrt{2})\exp(i\eta) & 0 \\ (1/\sqrt{2})\exp(-i\varphi) & 0 & 0 & (1/\sqrt{2})\exp(i\varphi) \end{bmatrix}. \tag{12}$$

If we take $\eta = \varphi = \pi/4$, the unitary transformation introduced above can break the transfer matrix into two 2×2 disconnected submatrices:

$$\hat{\mathbf{T}}_l = \mathbf{U}\mathbf{T}_l\mathbf{U}^+ = \begin{bmatrix} e^{i\alpha_l d_l}(J_l - iR_l) & e^{i\alpha_l d_l}(\theta_l - iR_l) & 0 & 0 \\ e^{i\alpha_l d_l}(\theta_l + iR_l) & e^{i\alpha_l d_l}(J_l + iR_l) & 0 & 0 \\ 0 & 0 & e^{-i\alpha_l d_l}(J_l - iR_l) & e^{-i\alpha_l d_l}(\theta_l - iR_l) \\ 0 & 0 & e^{-i\alpha_l d_l}(\theta_l + iR_l) & e^{-i\alpha_l d_l}(J_l + iR_l) \end{bmatrix}. \tag{13}$$

So after unitary transformation, equation (1) is reduced to

$$\begin{bmatrix} \tilde{A}_1^{l+1} \\ \tilde{B}_1^{l+1} \\ \tilde{B}_2^{l+1} \\ \tilde{A}_2^{l+1} \end{bmatrix} = \hat{\mathbf{T}}_l \begin{bmatrix} \tilde{A}_1^l \\ \tilde{B}_1^l \\ \tilde{B}_2^l \\ \tilde{A}_2^l \end{bmatrix} \tag{14}$$

where

$$\begin{bmatrix} \bar{A}_1^l \\ \bar{B}_1^l \\ \bar{B}_2^l \\ \bar{A}_2^l \end{bmatrix} = \mathbf{U} \begin{bmatrix} \tilde{A}_1^l \\ \tilde{B}_1^l \\ \tilde{B}_2^l \\ \tilde{A}_2^l \end{bmatrix} \tag{15}$$

and equation (11) is reduced to two equations

$$\begin{pmatrix} \bar{A}_1^{j+1} \\ 0 \end{pmatrix} = \begin{pmatrix} M_{11} & M_{12} \\ M_{21} & M_{22} \end{pmatrix} \begin{pmatrix} 0 \\ \bar{B}_1^0 \end{pmatrix} \tag{16}$$

$$\begin{pmatrix} 0 \\ \bar{A}_2^{j+1} \end{pmatrix} = \begin{pmatrix} M_{33} & M_{34} \\ M_{43} & M_{44} \end{pmatrix} \begin{pmatrix} \bar{B}_2^0 \\ 0 \end{pmatrix} \tag{17}$$

where M_{ij} $(i, j = 1\text{–}4)$ are the matrix elements of matrix $\mathbf{M}$ and

$$\mathbf{M} = \prod_{l=0}^{j} \hat{\mathbf{T}}_l. \tag{18}$$

From equations (17) and (18), we obtain

$$\bar{A}_1^{j+1} = M_{12}\bar{B}_1^0 \qquad M_{22}\bar{B}_1^0 = 0 \tag{19}$$

$$\bar{A}_2^{j+1} = M_{43}\bar{B}_2^0 \qquad M_{33}\bar{B}_2^0 = 0. \tag{20}$$

The conditions that there are non-trivial solutions are

$$M_{22} = 0 \qquad M_{33} = 0. \tag{21}$$

The energy spectra of type-II CQWs for either $\boldsymbol{K}_\perp = \mathbf{0}$ or $\boldsymbol{K}_\perp \neq \mathbf{0}$ can be determined by equation (21), and for each definite energy level the corresponding wavefunction can be obtained by means of equation (14).

3. Electric-field-induced evenly spaced energy spectrum and localisation of the wavefunctions

For type-II InAs/GaSb systems, when the electric field $F = 0$, the structure of the band edge can be expressed as

$$V_p(z) = V_s(z) = 0$$

when z is located in the InAs layers and as

$$V_p(z) = \Delta + \varepsilon_{InAs} = 560\ \text{meV}$$

$$V_s(z) = \Delta + \varepsilon_{GaSb} = 960\ \text{meV}$$

Table 1. The electron energy spectrum of type-II CQWs for $\boldsymbol{K}_\perp = \mathbf{0}$.

Label number of energy level	Energy (meV)
1	20.9581
2	50.9717
3	80.9734
4	110.9921
5	141.0013

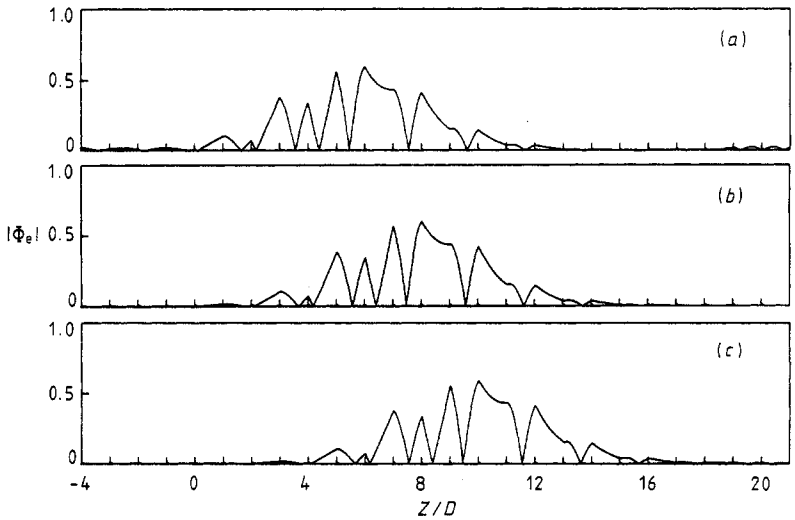

Figure 2. A plot of the moduli of electron envelope functions of type-II CQWs for $K_\perp = 0$ for energy levels E of (*a*) 20.9581 meV, (*b*) 50.9717 meV and (*c*) 80.9734 meV.

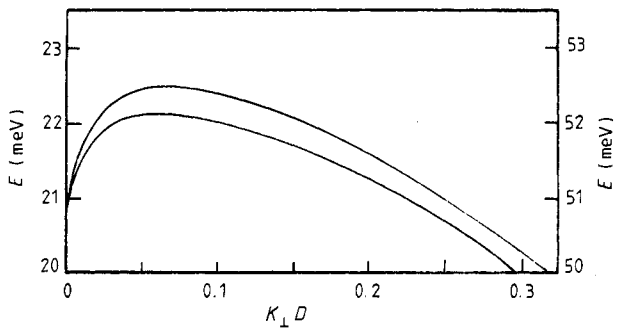

Figure 3. The variation in electron energies of type-II CQWs versus the wavevector $K_\perp$ for the lowest two energy levels.

when z is located in the GaSb layers, where ε_{InAs} and ε_{GaSb} are the forbidden gaps of InAs and GaSb, respectively, and $\Delta = 150$ meV is the overlap part of the CB of InAs and the VB of GaSb. Following [4], we take the Kane matrix element as

$$\prod = (\hbar/m_0)\langle iS|\hat{p}_z|Z\rangle = 1.035 \times 10^{-4} \text{ meV cm}.$$

We discuss here a CQW consisting of ten wells plus ten barriers and embedded between infinite potential barriers at both ends. A constant electric field F is applied along the growth axis Z. The other parameters in our numerical calculation are $F = 30$ kV cm^{-1}. The width D of the wells is equal to 50 Å. The width of barriers that separate the wells is the same as that of the wells. The sublayer number j_s of each well or each barrier is 15, i.e. the width of each sublayer is about 3.33 Å and the total number j_T of sublayers between the infinite barriers at both ends is 300.

The resulting electron energy spectrum of this system for $K_\perp = 0$ is listed in table 1. It is nearly an evenly spaced spectrum closely in accordance with the Wannier–Stark ladder formula [2]:

$$\varepsilon_\gamma = E_1 + \nu eF(2D) \qquad 0 \leqslant \nu \leqslant 10.$$

In figure 2, the moduli of electronic envelope functions that correspond to the energy levels listed in table 1 are plotted. It is seen that the envelope functions of type-II CQWs

also show electric-field-induced localisation. All the curves of these figures have nearly the same shape. If the curve in figure 2(*a*) is translated by a distance of $2D$ or $4D$, it will nearly coincide with the curves in figure 2(*b*) or 2(*c*).

In figure 3, the electron energies are plotted against $\boldsymbol{K}_\perp$ for the lowest two levels. The lower curve corresponds to the ground-state level, and the upper to the first excitation-state level. It turns out that the motion of electrons in Z direction is closely related to that in the x–y plane so that the dispersion relations have a non-parabolic shape. The lower the energy of a level, the more obvious is the non-parabolic shape that it displays. The energy value labelled at the longitudinal coordinate at the left-hand side of the figure is the energy value of the ground-state level, and that labelled on the right-hand side of the figure is the energy value of the first excitation-state level. In [3], we have discussed the dispersion relation of an infinite type-II semiconductor quasi-periodic superlattice in the absence of an electric field. There is some similarity between the dispersion curves in figure 3 and that in [3].

For type-II systems, the interaction between CB and VB is strong. When $\boldsymbol{K}_\perp \neq \boldsymbol{0}$, the hole energy spectrum obtained from a single-band envelope function equation as discussed in [1] is not reliable. An attempt to generalise the ATM to deal with holes in a degenerate valence band edge is under way.

For type-I GaAs/$Al_xGa_{1-x}As$ CQWs, we considered a six-well CQW in [2] by means of the ATM. The structure of the electron energy spectrum obtained by the non-consistent ATM is similar to that in [2]. The only difference between these structures is that each of the energy levels obtained by the non-consistent ATM is about 7.8 meV higher than that obtained by the piecewise-constant potential model, when we take the electric field F equal to 30 kV cm^{-1} and the widths D of both wells and barriers equal to 50 Å, i.e. the energy value is raised by taking account of the declination of band edges is nearly equal to $FD/2$ and the envelope functions obtained by the non-consistent ATM differ only slightly from those in [2]. However, the self-consistent results of the ATM for type-I CQWs yield obvious modifications to those in [2]. All the results of the self-consistent ATM, the electron and hole energy spectra, the envelope functions and the optical absorption coefficient, will be presented in a subsequent paper.

Acknowledgment

This research is supported by the National Science Foundation of China.

References

[1] Qin G 1989 *J. Phys.: Condens. Matter* **1** 7335
[2] Bleuse J, Bastard G and Voisin P 1988 *Phys. Rev. Lett.* **60** 220
[3] Qin G 1988 *J. Phys. C: Solid State Phys.* **21** 4989
[4] Altarelli M 1983 *Phys. Rev.* B **28** 842
[5] Bastard G 1982 *Phys. Rev.* B **25** 7584